PERGAMON

Acta mater. Vol. 47, No. 13, pp. 3695–3703, 1999

Printed in Great Britain
PII: S1359-6454(99)00192-5
1359-6454/99 $20.00 + 0.00

SOLUTE SEGREGATION AND ANTIPHASE BOUNDARY MOTION IN A B2 SINGLE PHASE

Q. WANG†‡ and L.-Q. CHEN

Department of Materials Science and Engineering, The Pennsylvania State University, University Park, PA 16802, U.S.A.

(Received 8 March 1999; accepted 15 June 1999)

Abstract—Solute segregation and antiphase boundary (APB) migration in a B2-ordered single phase were studied using computer simulations based on the microscopic master equations in the point approximation with both first- and second-neighbor pair interactions. It is shown that the degree of segregation at APBs is highly anisotropic; for the particular case of a cylindrical APB along the *z*-directions, it is found that maximum segregation occurs along the [1 1 0]-direction and is essentially zero along the [1 −1 0]-direction. Despite the strong segregation anisotropy, however, it is demonstrated that the decrease in the square of the radius of the cylindrical antiphase domain in single-phase B2 is linearly proportional to time, *t*. It is also shown that the mobility of an APB at a given temperature is strongly composition dependent. © *1999 Acta Metallurgica Inc. Published by Elsevier Science Ltd. All rights reserved.*

Keywords: Computer simulation; Segregation; Ordering; Microstructure; Binary alloy

1. INTRODUCTION

The migration of antiphase boundaries (APBs) in a B2-ordered single phase has been investigated both experimentally [1–5] and theoretically [6–9]. For example, Krzanowski and Allen [2–5] studied the effect of solute segregation on the APB migration in Fe-rich Fe–Al alloys and found that solute segregation at APBs dramatically reduced their mobilities. Recently, employing a continuum model derived from the Bragg–Williams model, Maugis [7] and Kirkaldy and Savva [9] demonstrated that there is solute segregation even at the stoichiometric composition of the B2 phase. Furthermore, they showed that the degree of segregation is highly anisotropic. This poses an interesting question of how the anisotropy of segregation may affect the antiphase domain morphology, and the mobility and kinetics of domain boundary migration. Within the B2 single-phase field, Allen and Cahn [1], Lifshitz [10], and Kirkaldy and Savva [9] assumed that the relationship between the APD (antiphase domain) size and time t is linear regardless of the composition. On the other hand, Dobretsov *et al.* [6] investigated the motion of APB in a B2-ordered single phase using computer simulations based on the thermally activated direct exchange model to describe inter-site jumps of atoms and mean-field approximation to account for the atom–atom correlation. They demonstrated that the strong segregation of the alloy majority component (e.g. the Fe in Fe-rich alloys) at the APB results in a time dependence of the mobility at non-stoichiometric compositions whereas it is independent of time at the stoichiometric composition. This implies that the linear relationship between the square of the antiphase domain radius and time is only true at the stoichiometric composition.

The main objective of this paper is to investigate the kinetics of APB migration in a B2-ordered single phase, in particular, the effect of segregation anisotropy and the effect of composition on the boundary kinetics and mobility. For this purpose, we developed a three-dimensional computer simulation model based on microscopic master equations using either the point or the pair approximations with a second-neighbor interaction model. In this model, the anisotropic solute segregation at a moving antiphase boundary is automatically taken into account and the effect of composition on the kinetics of domain coarsening can be systematically investigated.

2. MODEL

We consider a b.c.c. lattice whose unit cell is shown in Fig. 1. It is divided into two sublattices, a and b. These two sublattices are related by a lattice translation along the [1, 1, 1]-direction by a vector $a_0/2(111)$, where a_0 is the lattice constant of the conventional b.c.c. unit cell. In a b.c.c. binary alloy, A and B atoms can occupy either the a- or b-sublattice. Under a certain condition (temperature and

†To whom all correspondence should be addressed.
‡Present address: Sarnoff Corporation, 201 Washington Rd., CN5300, Princeton, NJ 08543, U.S.A.

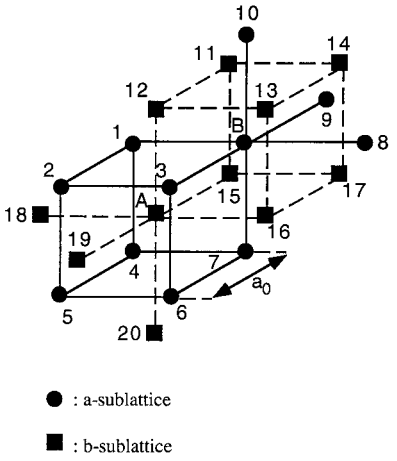

Fig. 1. The b.c.c. lattice is divided into two sublattices: a and b. The numbers 1–20 indicate the first and second neighbors of the pair AB or BA.

composition), A and B may have a preference to occupy either the a- or b-sublattice. For instance, for composition $c = 0.5$ at low temperatures, there is a higher probability of finding A atoms on the a-sublattice and B atoms on the b-sublattice, or vice versa, resulting in the so-called B2-ordered phase. At high temperatures, due to the mixing entropy effect, A (or B) atoms have the same probability of occupying a- and b-sublattices, forming a disordered phase.

In the microscopic master equation method, the structural state of an alloy at a given temperature and composition is described by a set of multiparticle distribution functions or cluster probabilities [11]. These multiparticle distribution functions satisfy the normalization conditions [12]; for example, summing the single-site distribution function $P_\alpha(\mathbf{r})$ [occupation probability of α-type atom (A or B) on site $\mathbf{r}$] over all lattice sites gives

$$\Sigma_{\mathbf{r}} P_\alpha(\mathbf{r}) = N_\alpha$$

where N_α is the total number of α-type atoms in the alloy.

Away from equilibrium all of the multiparticle distribution functions are at nonequilibrium and change with time as the atomic diffusion takes place on the lattice. For simplicity, we assumed a direct exchange mechanism for atomic diffusion and isothermal environment.

Let us consider a pair of interchange sites at $\mathbf{r}$ and a nearest-neighbor site, $\mathbf{r}+\delta$, and a set $\{\mathbf{x}\}$ of nearby sites on which atoms interact with the two interchanging atoms. If we have an A atom at $\mathbf{r}$, a B atom at $\mathbf{r}+\delta$, and a set of atoms $\{X\}$ at $\{\mathbf{x}\}$, we denote by $R_{\mathrm{AB}}(\{X\})$ the rate at which the AB pair interchanges under the influence of the set of neighboring atoms $\{X\}$ on $\{\mathbf{x}\}$ up to the second neighbors as shown by the numbers 1–20 in Fig. 1. Similarly, $R_{\mathrm{BA}}(\{X\})$ is the rate at which the BA pair will interchange under the same environment when the B atom is at $\mathbf{r}$, and the A atom is at $\mathbf{r}+\delta$. Then the rate of change of the probability that the site $\mathbf{r}$ occupied by an A atom is given by

$$\begin{aligned} \mathrm{d}P_{\mathrm{A}}(\mathbf{r})/\mathrm{d}t = {} & \Sigma_\delta \Sigma_{\{\mathbf{x}\}} P_{\mathrm{BA}}\{X\}(\mathbf{r}, \mathbf{r}+\delta, \{\mathbf{x}\}) \\ & R_{\mathrm{BA}}(\{X\}) - \Sigma_\delta \Sigma_{\{\mathbf{x}\}} P_{\mathrm{AB}}\{X\} \\ & (\mathbf{r}, \mathbf{r}+\delta, \{\mathbf{x}\}) R_{\mathrm{AB}}(\{X\}) \end{aligned} \tag{1}$$

where the first and second terms on the right-hand side are the average rates at which, on site $\mathbf{r}$, A atoms are appearing and disappearing, respectively; Σ_δ denotes the summation over all the nearest-neighbor sites, δ, of $\mathbf{r}$; and $P_{AB}\{X\}(\mathbf{r}, \mathbf{r}+\delta, \{\mathbf{x}\})$ is the probability of finding an A atom on $\mathbf{r}$, a B atom on $\mathbf{r}+\delta$, and the set $\{X\}$ on the neighboring sites $\{\mathbf{x}\}$ simultaneously. A similar equation can be written for $\mathrm{d}P_{\mathrm{B}}(\mathbf{r})/\mathrm{d}t$ since $P_A(\mathbf{r}) + P_B(\mathbf{r}) = 1$.

The reaction rate constant in equation (1) is calculated according to [11–13]

$$R_{\mathrm{AB}}(\{X\}) = \upsilon \exp\{-(U_0 + 1/2\Delta E)/k_{\mathrm{B}}T\} \tag{2}$$

where U_0 is the average activation energy for AB exchange, υ is the vibrational frequency associated with the AB exchange, ΔE is the energy difference before and after an atom exchange and dependent on the local atomic arrangements, T is the absolute temperature and k_{B} is Boltzmann's constant. Since $\upsilon \exp(-U_0/k_B T)$ occurs in all configurations, it can be combined with the time, t, in the kinetic equations to give a dimensionless time, t^*

$$t^* = t\upsilon \exp(-U_0/k_{\mathrm{B}}T). \tag{3}$$

Therefore, the time unit of t in our simulation is $1/\upsilon \exp(-U_0/k_B T)$ and the dimensionless time step is 0.01.

In order to carry out the sum on the right-hand side of equation (1), we need the joint probability distribution, $P_{AB}\{X\}(\mathbf{r}, \mathbf{r}+\delta, \{\mathbf{x}\})$. In this paper, we use the simplest point approximation by assuming statistical independence among occupation probabilities. In this approximation

$$\begin{aligned} P_{\mathrm{AB}}\{X\}(\mathbf{r}, \mathbf{r}+\delta, \{\mathbf{x}\}) & \\ = P_{\mathrm{A}}(\mathbf{r}) P_{\mathrm{B}}(\mathbf{r}+\delta) P_{X1}(\mathbf{x}1) P_{X2}(\mathbf{x}2) & \\ \ldots\ P_{Xn}(\mathbf{x}n) & \end{aligned} \tag{4}$$

where $\mathbf{x}1, \ldots, \mathbf{x}n$ are the individual sites in the set of neighboring sites around the pair, $\mathbf{r}$ and $\mathbf{r}+\delta$, and $X1, \ldots, Xn$ are the types of atoms occupying those sites.

The summation on the right-hand side of equation (1) is over all possible arrangements of A and B atoms on the sites which influence the atomic interchange at $\mathbf{r}$ and $\mathbf{r}+\delta$. For the b.c.c. binary alloy with a second-neighbor interaction model (Fig. 1), there are a total of 2^{20} possible terms in the summation. For each of the 2^{20} different configurations, the rate constants R_{AB} and R_{BA} have to

be calculated. The number of configurations will increase dramatically if a longer range interaction model is employed. However, in the point approximation, it is computationally much more efficient to replace the sum over products of individual single-site probabilities using the product of sums over A and B [12, 13], i.e.

$$\begin{aligned}
&\Sigma_{\{\mathbf{x}\}} P_{\mathrm{AB}}\{\mathbf{x}\}(\mathbf{r}, \mathbf{r}+\delta, \{\mathbf{x}\}) R_{\mathrm{AB}}(\{X\}) \\
&\quad = P_{\mathrm{A}}(\mathbf{r}) P_{\mathrm{B}}(\mathbf{r}+\delta)\big\{P_{\mathrm{A}}(1) \\
&\quad \exp[-(V^1_{\mathrm{AB}} - V^1_{\mathrm{AA}})/2k_{\mathrm{B}}T] + P_{\mathrm{B}}(1) \\
&\quad \exp[-(V^1_{\mathrm{BB}} - V^1_{\mathrm{BA}})/2k_{\mathrm{B}}T]\big\} \\
&\qquad \ldots \{P_{\mathrm{A}}(20)\exp[-(V^1_{\mathrm{AB}} - V^1_{\mathrm{AA}})/2k_{\mathrm{B}}T] \\
&\qquad\quad + P_{\mathrm{B}}(20)\exp[-(V^1_{\mathrm{BB}} - V^1_{\mathrm{BA}})/2k_{\mathrm{B}}T]\}
\end{aligned} \tag{5}$$

where $P_{\mathrm{A}}(k)$ and $P_{\mathrm{B}}(k)$, $k = 1, \ldots, 20$, are the values of single-site distribution functions P_{A} and P_{B} at site k around the pair $\mathbf{r}$ and $\mathbf{r}+\delta$, and the V^n_{AA} is defined as the nth neighbor interaction between A and A atoms and the same for A–B and B–B.

To solve the kinetic equations, we apply the simple Euler technique

$$P_{\mathrm{A}}(\mathbf{r}, t+\Delta t) = P_{\mathrm{A}}(\mathbf{r}, t) + \mathrm{d}P_{\mathrm{A}}(\mathbf{r})/\mathrm{d}t\,\Delta t. \tag{6}$$

In the traditional Bragg–Williams mean-field approximation the phase diagram for the b.c.c. binary alloy can be calculated [14]. The bond energies are chosen to be $V^1_{\mathrm{AA}} = 1.0$, $V^1_{\mathrm{AB}} = 0.0$, $V^1_{\mathrm{BB}} = 0.0$, and $V^2_{\mathrm{AA}} = -0.86$, $V^2_{\mathrm{AB}} = 0.0$, $V^2_{\mathrm{BB}} = 0.0$. Therefore, the effective interaction energies are given by

$$\begin{aligned}
w_1 &= V^1_{\mathrm{AA}} + V^1_{\mathrm{BB}} - 2V^1_{\mathrm{AB}} = 1.0 \\
w_2 &= V^2_{\mathrm{AA}} + V^2_{\mathrm{BB}} - 2V^2_{\mathrm{AB}} = -0.86
\end{aligned} \tag{7}$$

where w_1 and w_2 are the first- and second-neighbor effective interchange energies and the interactions beyond the second coordination shell are neglected. The free energy per lattice site can then be obtained for the B2 phase of the b.c.c. structure as follows:

$$\begin{aligned}
F = 1/2\{&c^2 V_0 + (\eta)^2 V_1 + k_{\mathrm{B}}T[(c+\eta)\ln(c+\eta) \\
&+ (1-c-\eta)\ln(1-c-\eta) + (c-\eta)\ln(c-\eta) \\
&+ (1-c+\eta)\ln(1-c+\eta)]\}
\end{aligned} \tag{8}$$

where c is the mole fraction of component A, η is the order parameter, $V_0 = 7w_1 + 6w_2$ and $V_1 = -7w_1 + 7w_2$.

The conventional common-tangent construction for the F vs c curves at different temperatures determines the equilibrium compositions of the disordered D phase and the ordered B2 phase and allow one to draw the solubility lines. Therefore, the phase boundary and spinodal curves for the point approximation are calculated using equation (8) and are presented in Fig. 2. There are three regions in the phase diagram: B2-ordered phase (B2), disordered phase (D) and two-phase coexistence (B2 + D), and the solid lines are the phase boundaries of the low temperature two-phase field, dot-dashed line is the ordering transition line of the second kind extended into the D + B2 field, thin line is the stable ordering transition line of the second kind, dotted line is the conditional spinodal and letters X represent the alloy compositions and temperatures chosen for the computer simulation. Reduced temperature $T^* = k_B T/|V_1|$ is used in the phase diagram representation. This phase diagram is topologically very similar to the upper part of the Fe–Al diagram describing the two-phase field, the disordered + ordered B2 phase [15].

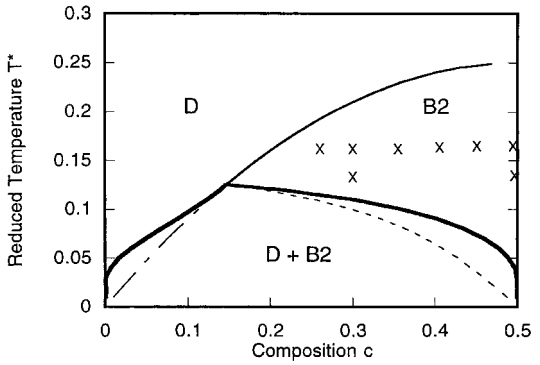

Fig. 2. The calculated phase diagram for b.c.c. alloy in a point approximation with interactions up to second neighbors.

In order to characterize the B2-ordered phase, we defined the long-range order parameter η in terms of single-site occupation probabilities using $\eta(\mathbf{r}) = [P^{\mathrm{a}}_{\mathrm{A}}(\mathbf{r}) - P^{\mathrm{b}}_{\mathrm{A}}(\mathbf{r})]/2$, where a and b label the two sublattices. The corresponding local composition is defined as $c(\mathbf{r}) = [P^{\mathrm{a}}_{\mathrm{A}}(\mathbf{r}) + P^{\mathrm{b}}_{\mathrm{A}}(\mathbf{r})]/2$. The local solute segregation is measured by defining $s(\mathbf{r}) = c(\mathbf{r}) - c_0$, where c_0 is the average composition of the system.

3. RESULTS AND DISCUSSION

3.1. Initial configuration of APB

We employed a simulation supercell $64 \times 64 \times 2$ conventional b.c.c. unit cells with two lattice sites per unit cell (Fig. 1). Periodic boundary conditions are applied along all three directions. We considered a cylindrical antiphase domain with a radius $R = 30$ (unit is lattice constant). The initial condition is generated as follows: inside the cylinder, $P^{\mathrm{a}}_{\mathrm{A}}(\mathbf{r})$ and $P^{\mathrm{b}}_{\mathrm{A}}(\mathbf{r})$ are, respectively assigned high and low values corresponding to the equilibrium B2-ordered single phase at the temperature and composition of interest, and outside, $P^{\mathrm{a}}_{\mathrm{A}}(\mathbf{r})$ and $P^{\mathrm{b}}_{\mathrm{A}}(\mathbf{r})$ are assigned low and high values, respectively.

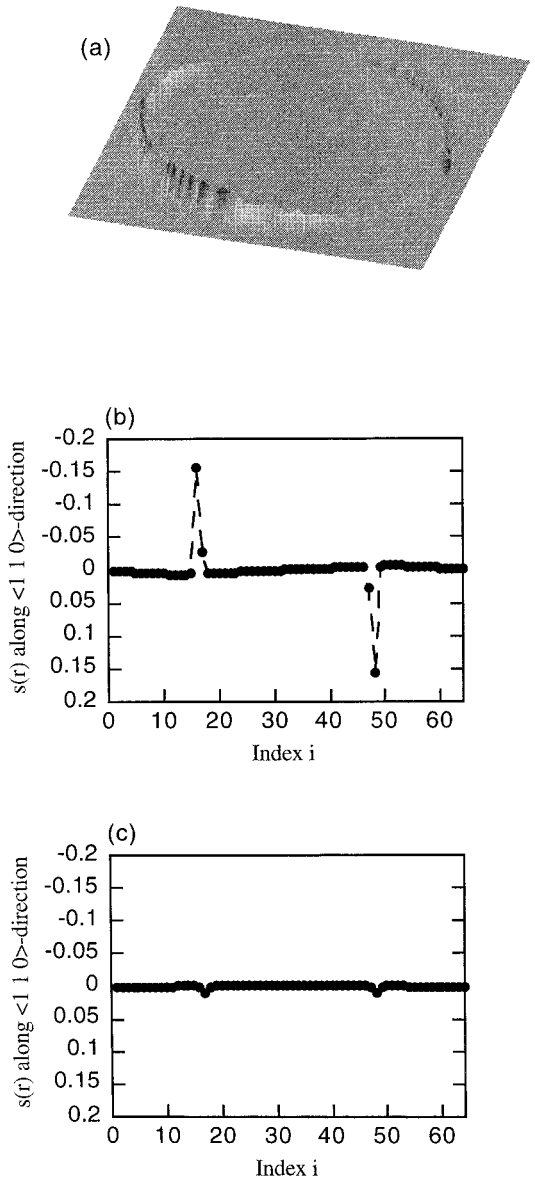

Fig. 3. The profile of concentration segregation for the stoichiometric alloy at $T^* = 0.14$: (a) $t^* = 37.5$ (i.e. $t = 37.5$ unit); (b) the cross section along the [1, 1, 0]-direction; (c) the cross section along the [1, −1, 0]-direction.

3.2. Stoichiometric composition ($c = 0.5$)

From Fig. 2 it can be seen that for composition $c = 0.5$, below the order–disorder transition critical reduced temperature $T^* = 0.25$, there is only a single B2-ordered phase. To study the APB migration, T^* is chosen to be below the order–disorder transition temperature for the B2-ordered phase. The solute segregation profile at $T^* = 0.14$ and time $t^* = 37.5$ unit is presented in Fig. 3(a). It can be seen that the amplitude of compositional segregation at the APB is highly orientation dependent and can be either positive or negative. The maximum segregation in amplitude occurs along the [1, 1, 0]-direction as shown in Fig. 3(b) and no segregation along the [1, −1, 0]-direction as shown in Fig. 3(c). Therefore, anisotropic segregation at the APB is automatically predicted by our simulations.

In order to describe the degree of anisotropy, we defined a parameter, *sd*, as

$$sd = |\max s(\mathbf{r}) - \min s(\mathbf{r})|.$$

The parameter *sd* is a function of temperature and composition. In the stoichiometric alloy with $c = 0.5$, the values of *sd* at different temperatures are listed in Table 1. The segregation at APB shows stronger anisotropy ($sd = 0.445$) at a lower temperature ($T^* = 0.123$) than $sd = 0.085$ at a higher temperature ($T^* = 0.222$).

The size of APD (the area of the circular domain in the x–y cross section) as a function of time t^* is plotted in Fig. 4, where $S(\text{size of APD}) = \pi R^2$, $\pi = 3.14$ and R is the radius of the circular domain. The equation

$$R^m(t^*) - R_0^m(t^* = 0) = kt^* \tag{9}$$

is used to fit the data and the best fitting gives $m = 2.0$, which indicates a linear relationship between S and t^*. The slope (k) of the linear function is proportional to the mobility of the circular APB. Therefore, it is interesting that despite the anisotropic segregation, the domain remains circular on the x–y cross section through the entire simulation and the APD size decreases linearly with time.

By examining the segregation profile, it is found that the width of the segregation region ranges from two to five lattice constants. For the B2-ordered phase in the Fe–Al alloy, the lattice constant a_0 is about 4.2 Å. Using this value as a typical value for the lattice parameter, the width predicted from our model is about 8.4–21 Å. Krzanowski and Allen indicated from their experimental measurements that the width of segregation in the B2 with 75% Fe is about 10–13 Å [2–4]. Although we employed a model binary alloy and without any attempt to fit our interaction parameters to the Fe–Al system, our prediction on the segregation width in the B2-ordered single-phase region seems to be of a similar order of magnitude as experimental measurements in the B2-ordered phase. The width of the segregation region at various temperatures is listed in Table 1 for $c = 0.5$.

3.3. Non-stoichiometric composition ($c = 0.3$)

At this composition, the alloy is an ordered B2 phase at temperatures higher than $T^* = 0.11$, or a two-phase (B2 + D) coexistence at temperatures lower than $T^* = 0.11$. We discuss the APB motion within the B2-ordered single-phase region.

At $T^* = 0.14$, the alloy is a B2 single phase. A snapshot of the segregation profile is shown in Fig.

Table 1. The maximum segregation ($s(\mathbf{r})$), degree of segregation (sd), the slope in the plot of area vs time, and the width of segregation region as a function of temperature for $c = 0.5$ at $t^* = 37.5$

T^*	Maximum $s(\mathbf{r})$	sd	Slope	Width (Å)
0.123	0.222	0.445	−16.6	8.40
0.140	0.162	0.323	−17.5	12.6
0.148	0.128	0.255	−17.7	12.6
0.164	0.098	0.197	−17.8	12.6
0.189	0.078	0.155	−17.8	12.6
0.206	0.062	0.124	−17.7	16.8
0.222	0.043	0.085	−17.5	21.0

5(a), where the magnitude of segregation is scaled by gray-levels with the completely bright scale representing the maximum segregation and the dark scale representing no segregation. The corresponding cross section along the [1, 1, 0]-direction is shown in Fig. 5(b), where the asymmetric amplitude can be clearly seen. The cross section along the [1, −1, 0]-direction is presented in Fig. 5(c), which shows a non-zero concentration segregation. The anisotropy degree, sd, is 0.160 at this composition and temperature, which is less than that in the stoichiometric alloy at the same temperature. The degree of anisotropy, sd, at different temperatures, is listed in Table 2. When the alloy is in the single B2-ordered phase region, Table 2 shows that the width (16.8–21 Å) of segregation at non-stoichiometric composition is of the same order as that (8.2–21 Å) at stoichiometric composition, although the actual values are slightly greater on average in the former than in the latter.

For this non-stoichiometric composition ($c = 0.3$), the size of APD and time t^* deviates slightly from the linear relationship. Using the same fitting procedure as for the stoichiometric alloy, the best fitting gives index $m = 1.98$ at $T^* = 0.140$, which implies the γ in $S = k(t^*)^{\gamma}$ is slightly larger than 1.0. At temperature $T^* = 0.164$, similar fittings have been systematically conducted for different compositions, e.g. $c = 0.25$, 0.3, 0.35, 0.4, 0.45 and 0.5, and on both simulation systems, i.e. $64 \times 64 \times 2$ and $128 \times 128 \times 2$, in order to see the size effect of the computer simulation system. For the $128 \times 128 \times 2$ system, the initial radius of the circular antiphase domain is 60 unit. The best fittings from both simulation systems give similar values for the exponent m listed in Table 3. This implies that the relationship of S–t^* at non-stoichiometric alloy is no longer rigorously linear, although it is very close to being linear. It is quite surprising that the values for m are slightly less than 2.0 for all the non-stoichiometric alloys in the single B2-ordered phase; the reason that the exponent can be less than 2.0 remains to be investigated.

The linear behavior of the s–t relationship can be written as the linear relationship between velocity of shrinkage of APD ($\mathrm{d}R/\mathrm{d}t$) and the curvature of

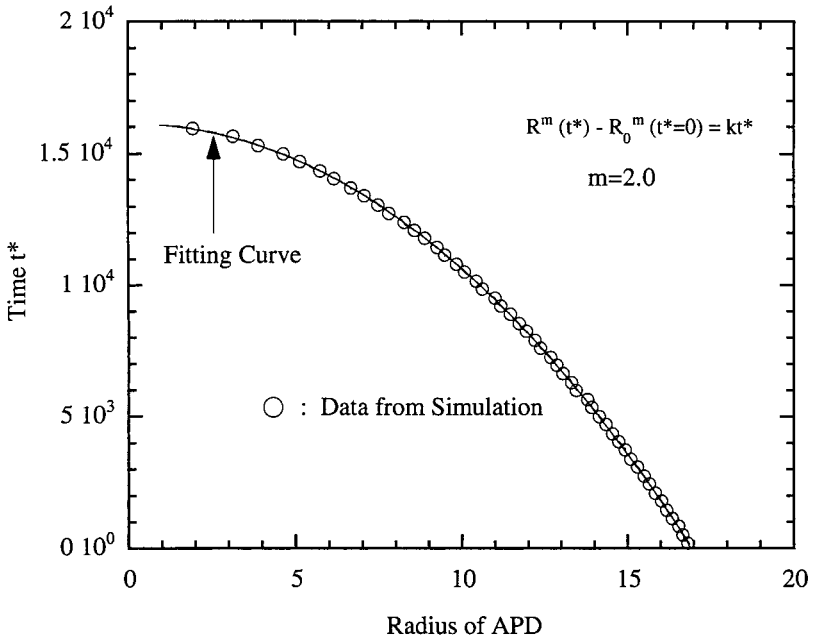

Fig. 4. The linear relationship between size (πR^2) of APD and time t^* in the stoichiometric alloy at $T^* = 0.14$.

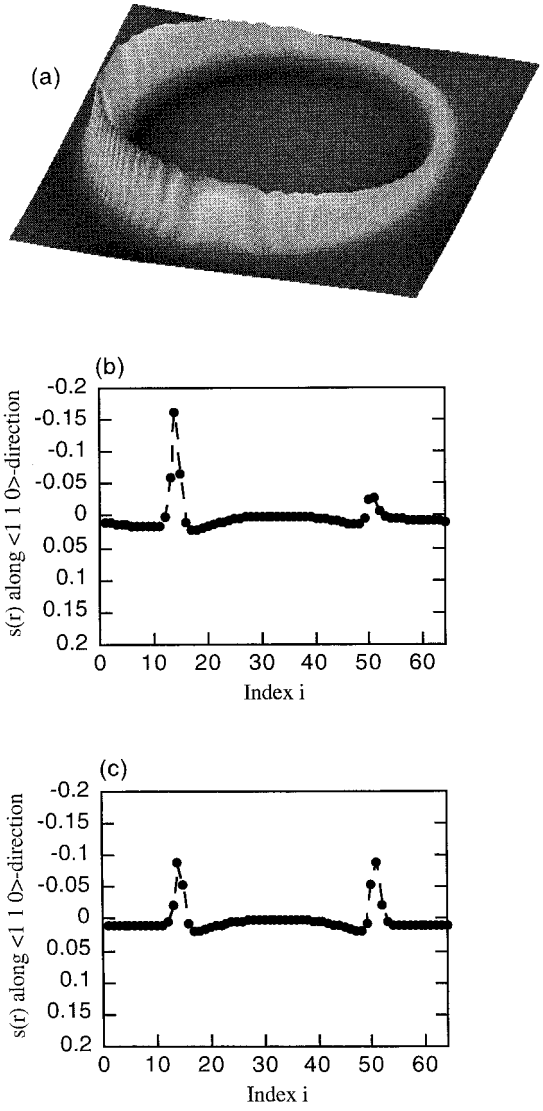

Fig. 5. The profile of concentration segregation for non-stoichiometric alloy ($c = 0.3$) at $T^* = 0.14$: (a) $t^* = 200$ (i.e. $t = 200$ unit); (b) the cross section along the [1, 1, 0]-direction; (c) the cross section along the [1, −1, 0]-direction.

APB ($1/R$), which is

$$dR/dt = \kappa/R$$

where κ is the mobility. The relationship was proposed by Allen and Cahn [1] based on their experimental observations in a single B2-phase region. They showed that it is valid regardless of composition, and supported by Lifshitz [10] and Kirkaldy and Savva [9] from different models. The only difference among their predictions about this linear relationship is the function of κ with temperature. However, our computer simulations showed that the relationship is only approximately linear at non-stoichiometric compositions.

The little deviation of m from 2.0 at non-stoichiometric alloy might be due to the different degree of B2 order from the stoichiometric alloy. This different order degree results in a slightly different segregation across the APBs and different curvature of compositional profile within the APD area. As compared in Fig. 6, the compositional profile within the domain area of stoichiometric alloy is more flat or homogeneous than that of the non-stoichiometric alloy. It suggests that the segregation might be curvature dependent and the curvature may drive a small flow flex of matter within the domain, from the boundary region to the center area [16].

A simulation with random initial condition, where atom A or B was randomly distributed on each lattice site, was conducted to see the effect of initial condition on the solute segregation profiles. Starting with this random initial condition, the simulation gave a multidomain distribution with different shape for each domain. The segregation profiles across the APB around each domain showed a greater segregation along the [1, 1, 0]-direction and less segregation along the [1, −1, 0]-direction. This is similar to the observation at the circular APB case. This might imply that the choice of the initial condition was arbitrary and would not change the preference of segregation along the [1, 1, 0]-direction of the B2 single phase in a b.c.c.-based binary alloy.

Does the local definition of order parameter and composition affect the segregation profiles across the APB? In order to answer this question, two different local definitions have been tested. The first case is just what we used in this paper. In the second case, five points were taken into account, one $P_A^a(\mathbf{r})$ and its four nearest neighbors, $P_A^b(\mathbf{r}_1)$, $P_A^b(\mathbf{r}_2)$, $P_A^b(\mathbf{r}_3)$, and $P_A^b(\mathbf{r}_4)$, and the local composition and order parameter were then, respectively defined as

$$C(\mathbf{r}) = \{P_A^a(\mathbf{r}) + (P_A^b(\mathbf{r}_1) + P_A^b(\mathbf{r}_2) + P_A^b(\mathbf{r}_3) + P_A^b(\mathbf{r}_4))/4\}/2$$

Table 2. The maximum segregation ($s(\mathbf{r})$), degree of segregation (sd), and the width of segregation region as a function of temperature for $c = 0.3$ at $t^* = 200$

T^*	Maximum $s(\mathbf{r})$	sd	Width (Å)
0.123	0.193	0.142	21.0
0.140	0.163	0.160	16.8
0.148	0.131	0.117	21.0
0.164	0.110	0.101	21.0
0.181	0.063	0.060	21.0

Table 3. The values for m of equation (4) at temperature $T^* = 0.164$ and different compositions: (a) for $64 \times 64 \times 2$; (b) for $128 \times 128 \times 2$

Composition	Index m (a)	Index m (b)
0.25	1.86	1.85
0.30	1.94	1.90
0.35	1.88	1.85
0.40	1.86	1.92
0.45	1.95	1.98
0.50	2.00	2.00

and

$$\eta(\mathbf{r}) = \{P_A^a(\mathbf{r}) - (P_A^b(\mathbf{r}_1) + P_A^b(\mathbf{r}_2) + P_A^b(\mathbf{r}_3) + P_A^b(\mathbf{r}_4))/4\}/2.$$

The second definition gave a very similar segregation profile across the circular APB to those shown in Fig. 3(a) obtained by the first definition. The similarities between these simulation results from the two different local definitions could show that the difference in local definition of order parameter or composition has no effect on the segre-

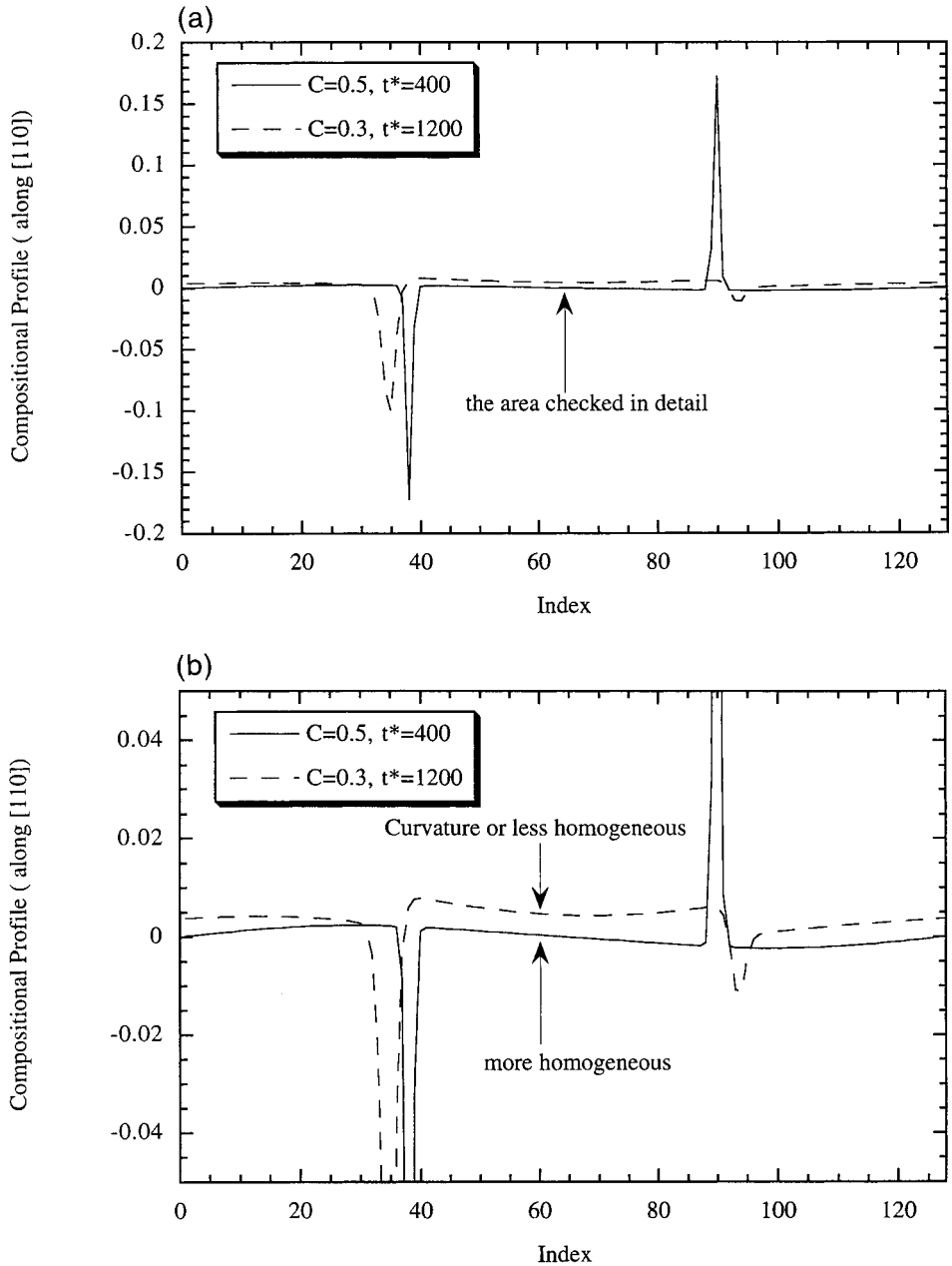

Fig. 6. The comparison of compositional profiles along the [1, 1, 0]-direction for both the stoichiometric ($c = 0.5$) and non-stoichiometric ($c = 0.3$) alloys at $T^* = 0.164$ with $128 \times 128 \times 2$ unit cells. (a) Overview of the compositional profiles. (b) Comparison of the curvatures in detail.

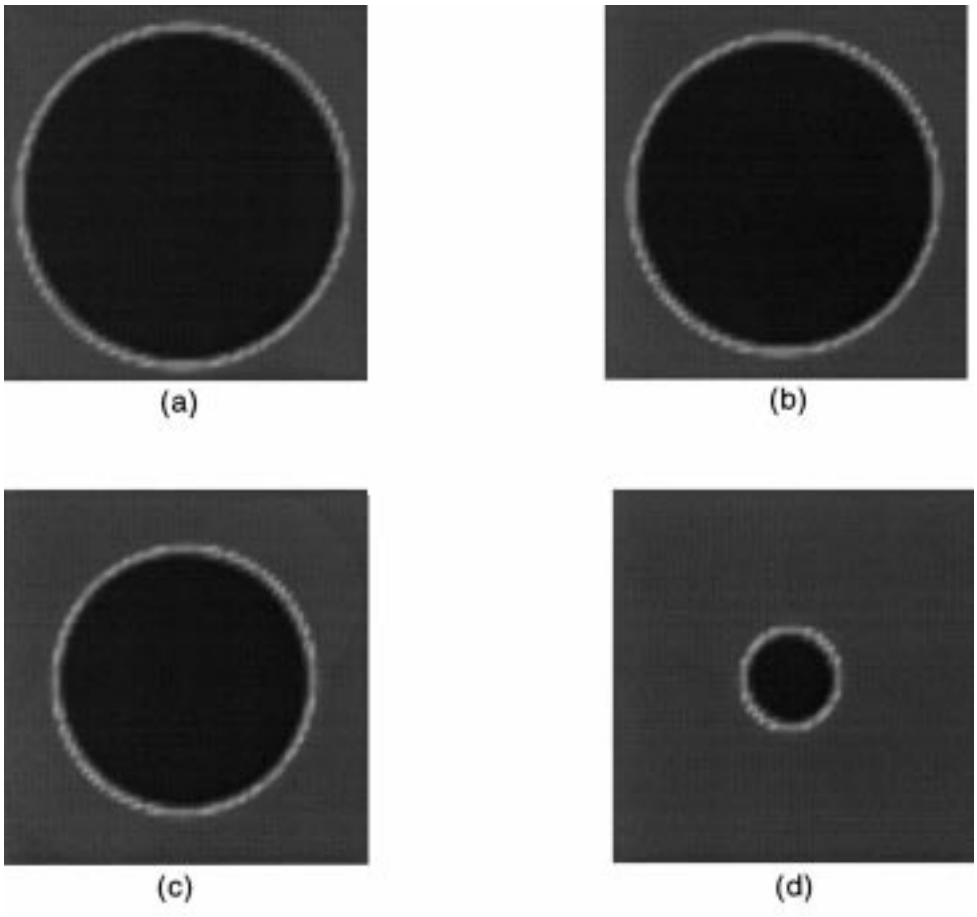

Fig. 7. The time-evolution of the circular APB at composition $c = 0.5$, temperature $T^* = 0.14$ and the different time snapshots t^* of: (a) 18.75; (b) 37.5; (c) 75; (d) 150.

gation profiles. Therefore, we used, in this paper, the first definition due to its simplicity.

The order parameter around the circular APB held the circular shape all the time until the size of the antiphase domain shrank to zero, as shown in Fig. 7.

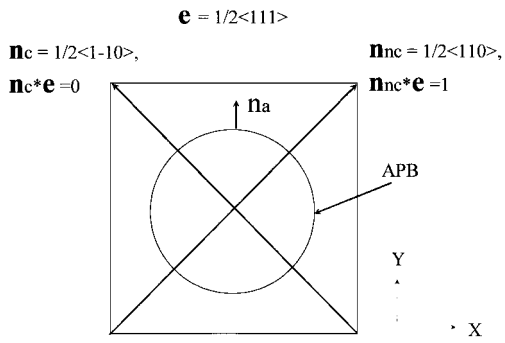

Fig. 8. The schematic representation of the relationship between the translation vector $\mathbf{e} = 1/2[1, 1, 1]$ of the B2 phase of the b.c.c. structure and the normal vector $\mathbf{n}_a$ of APB. Two special normal vectors of APB are $\mathbf{n}_{nc} = 1/2[1, 1, 0]$ and $\mathbf{n}_c = 1/2[1, -1, 0]$, which represent the non-conservative direction with $|\mathbf{n}^*_{nc}\mathbf{e}|$ = maximum and conservative direction with $\mathbf{n}^*_c\mathbf{e} = 0$, respectively.

The magnitude of solute segregation appears larger along the $1/2[1, 1, 0]$-direction than along the $1/2[1, -1, 0]$-direction in the two-dimensional case and the phenomenon was attributed to the non-conservative and conservative nature of these two directions. As shown in Fig. 8, the $1/2[1, 1, 0]$-direction has a maximum dot product with the translation vector $\mathbf{e} = 1/2[1, 1, 1]$ of the B2 phase of the b.c.c. structure and the $1/2[1, -1, 0]$-direction has zero dot product with the translation vector. The APB with normal vector of $1/2[1, 1, 0]$ is then called a non-conservative APB and that with normal vector of $1/2[1, -1, 0]$ is called a conservative APB. The non-conservative APB shows a difference in solute segregation from the conservative APB due to the non-zero dot product with the translation vector. The zero dot product between the conservation APB and the translation vector results in the disappearance of the first derivative cross terms between the order parameter and the concentration in free-energy formula which was suggested to be responsible for the formation of solute segregation across the APB of the B2 phase in the b.c.c. structure [7].

In one dimension, to be more specific, the atomic distribution would look like ABABAB|BABABABA|ABABAB in order to have the overall composition 0.5 when $c = 0.5$, where | represents the antiphase domain boundary. Seemingly, in general, there is no two-fold symmetry with 180 degree rotation that should exist for an ABABAB ordered structure in one dimension. However, by looking very carefully at each ordered domain, the two-fold structural symmetry of the B2-ordered phase still holds. This two-fold structural symmetry within each B2-ordered phase domain is also true in two-dimensional simulations. Since the APD boundaries are only a very small portion of the whole system, the symmetry of the system is then determined by the symmetry of each ordered domain. So, the two-fold symmetry of the B2-ordered phase holds for the whole system.

4. SUMMARY AND CONCLUSIONS

Using the microscopic master equation in point approximation with atomic interactions up to second neighbor, the kinetics and thermodynamics of a cylindrical (with a circular projection on the x–y two-dimensional plane) antiphase boundary in a b.c.c.-based A_cB_{1-c} alloy were studied for both stoichiometric ($c = 0.5$) and non-stoichiometric ($c = 0.3$) composition. Particularly, the studies were conducted on the local compositional profile across APB, the relationship between size of antiphase domain (APD) and time t^*, the mobility of APB, and the width of the compositional segregation area. Based on the results obtained and discussion, we make the following conclusions:

1. The local compositional profile is highly anisotropic at APB in stoichiometric alloy and a strong concentration segregation occurs at the APB.
2. Comparing with the stoichiometric alloy, the segregation anisotropy at APB in the non-stoichiometric alloy is weaker.
3. The relationship between size of APD and time t^* is a linear function within the single B2-ordered phase region at the stoichiometric composition and it becomes slightly nonlinear at non-stoichiometric compositions.
4. The two-fold symmetry of B2-ordered phase of b.c.c.-based A_cB_{1-c} alloy still holds during the APD migration.

Acknowledgements—This work is supported by ARPA/NIST program on mathematical modeling of microstructural evolution in advanced alloys and by ONR under Grant No. 00014-95-1-0577. The computations were partly performed on the CRAY at the Pittsburgh Supercomputing Center and CPU time was provided by the Center under Grant Nos. 940015P and 960007p.

REFERENCES

1. Allen, S. M. and Cahn, J. W., *Acta metall.*, 1979, **27**, 1085.
2. Krzanowski, J. E. and Allen, S. M., *Acta metall.*, 1983, **31**, 213.
3. Krzanowski, J. E. and Allen, S. M., *Surf. Sci.*, 1984, **144**, 153.
4. Krzanowski, J. E. and Allen, S. M., *Acta metall.*, 1986, **34**, 1035.
5. Krzanowski, J. E. and Allen, S. M., *Acta metall.*, 1986, **31**, 1045.
6. Dobretsov, V. Y., Martin, G., Soisson, F. and Vaks, V. G., *Europhys. Lett.*, 1995, **31**, 417.
7. Maugis, P., *Phys. Rev. B*, 1996, **53**, 5276.
8. Ohta, T., Kawasaki, K., Sato, A. and Enomoto, Y., *Phys. Lett. A*, 1987, **126**, 93.
9. Kirkaldy, J. S. and Savva, G., *J. appl. Phys.*, submitted.
10. Lifshitz, L. M., *Soviet Phys., JETP*, 1962, **15**, 939.
11. Vineyard, G. H., *Phys. Rev.*, 1956, **102**, 981.
12. Chen, L. Q. and Simmons, J. A., *Acta metall.*, 1994, **42**, 2943.
13. Geng, C. W. and Chen, L. Q., *Surf. Sci.*, 1996, **355**, 299.
14. Chen, L. Q. and Khachaturyan, A. G., *Acta metall.*, 1991, **39**, 2533.
15. Swann, P. R., Duff, W. R. and Fisher, R. M., *Metall. Trans.*, 1972, **3**, 409.
16. Chen, L. Q. and Wang, Q., *Scripta mater.*, 1998, **39**, 1113.